


Synthesis and Application of a Near-Infrared Light-Emitting Fluorescent Probe for Specific Imaging of Cancer Cells with High Sensitivity and Selectivity

Shaoguang Li¹, Zhan Lin¹, Haobo Chen¹, Qiu Luo¹, Shengnan Han¹, Kunlong Huang¹, Ruichan Chen¹, Yuying Zhan¹, Bing Chen², Hong Yao¹⁻³ 

¹Department of Pharmaceutical Analysis, School of Pharmacy, Fujian Medical University, Fuzhou, Fujian, People's Republic of China; ²Higher Educational Key Laboratory for Nano Biomedical Technology of Fujian Province, Fujian Medical University, Fuzhou, Fujian, People's Republic of China; ³Fujian Key Laboratory of Drug Target Discovery and Structural and Functional Research, Fujian Medical University, Fuzhou, Fujian, People's Republic of China

Correspondence: Shaoguang Li; Hong Yao, Department of Pharmaceutical Analysis, School of Pharmacy, Fujian Medical University, 1 Xue Yuan Road, University Town, Fuzhou, Fujian, 350122, People's Republic of China, Email lsg941@126.com; yauhung@126.com

Background: The preclinical diagnosis of tumors is of great significance to cancer treatment. Near-infrared fluorescence imaging technology is promising for the in-situ detection of tumors with high sensitivity.

Methods: Here, a fluorescent probe was synthesized on the basis of Au nanoclusters with near-infrared light emission and applied to fluorescent cancer cell labeling. Near-infrared methionine-N-Hydroxy succinimide Au nanoclusters (Met-NHs-AuNCs) were prepared successfully by one-pot synthesis using Au nanoclusters, methionine, and N-Hydroxy succinimide as frameworks, reductants, and stabilizers, respectively. The specific fluorescence imaging of tumor cells or tissues by fluorescent probe was studied on the basis of SYBYL Surflex-DOCK simulation model of LAT1 active site of overexpressed receptor on cancer cell surface. The results showed that Met-NHs-AuNCs interacted with the surface of LAT1, and C_Score scored the conformation of the probe and LAT1 as five.

Results: Characterization and in vitro experiments were conducted to explore the Met-NHs-AuNCs targeted uptake of cancer cells. The prepared near-infrared fluorescent probe (Met-NHs-AuNCs) can specifically recognize the overexpression of L-type amino acid transporter 1 (LAT1) in cancer cells so that it can show red fluorescence in cancer cells. Meanwhile, normal cells (H9c2) have no fluorescence.

Conclusion: The fluorescent probe demonstrates the power of targeting and imaging cancer cells.

Keywords: Au nanoclusters, fluorescence imaging, cancer cell imaging, molecular docking

Introduction

Epidemiological studies have shown that the incidence and mortality of cancer have been increasing in recent decades.^{1,2} Thus, the early screening of people who are at high risk of cancer can detect tumors in time and increase their chances of receiving treatment and cure.³ Therefore, the use of sensitive and specific detection techniques to locate solid tumors is the first and indispensable step in the treatment of cancer patients.⁴

With the continuous development of optical imaging technology for decades, it has been widely used in the preclinical diagnosis and treatment of cancer in biomedical research.⁵⁻⁸ Nanomaterials for optical imaging, such as nano clusters,⁹ silicon dioxide, carbon dots and magnetic materials,^{10,11} have always been the focus of cancer diagnosis research because of their uniqueness.¹² The intrinsic optical properties of nanoparticles make them quickly become the best choice for various cell imaging modes.¹³ Nanoparticles usually combine with suitable targeted ligands on the particle surface to form luminescent materials with different emission wavelengths because of their high sensitivity, small size, and composition. Among them, Au nanoclusters (AuNCs) have become a hot research fields of cancer cell imaging applications because of their ultra-fine size, biocompatibility (eg, bioinertia and low cytotoxicity),¹⁴ unique and highly adjustable optical properties, and photostability. However, the most

challenging issues for large-scale application of imaging Au nanoclusters of cancer cells are their specificity and sensitivity. In tumor diagnosis, distinguishing cancer cells from normal cells accurately is very important.^{15,16}

To improve the sensitivity and selectivity of tumor imaging, it is the most ideal method to develop targeted tumor fluorescent imaging materials that can specifically recognize the entry of overexpressed receptors into tumor cells. In recent years, a variety of functional small molecule dyes have been developed for specific targeted fluorescence imaging of specific tissues or receptors.^{17–22} For example, Wang et al successfully synthesized a CP-IRT Nir-II molecular imaging probe with high affinity and specificity by coupling CD133 Targeting peptide CP with Nir-II fluorophore IRT.²³ Wang et al synthesized cyanine dyes with three organic compounds, namely, Pyridinium salt, the α -diketone compound, and potassium tert-butoxide. The cyanine dye can distinguish normal cells from cancer cells successfully.²⁴ These fluorescent imaging materials that target cancer cells show good application prospects. However, the complicated synthesis conditions and synthetic after tedious purification process and other issues for the development of Au nanomaterials have certain challenges. Therefore, fluorescent dye ligands must be explored with simple, safe, and rapid synthesis. Due to the rapidly proliferating nature of cancer cells, a large supply of sugars, amino acids, and other nutrients is necessary for their continued growth. In order to obtain adequate nutrition, nutrient transporters on the surface of tumor cells are upregulated.^{25,26} In particular, the L-type amino acid transporter (LAT1) is of interest and widespread due to its cancer-specific expression, while it is also an essential amino acid transporter,²⁷ which is poorly expressed or absent in most non-cancerous tissues.²⁸ Therefore, many anti-tumor drugs have chosen LAT1 as a target to treat cancer.^{25,29,30} From this point of view, LAT1 can also be a promising method for cancer diagnosis.

As shown in Figure 1, based on the principle of AuNP colorimetry, the colorimetric sensor was constructed with methionine and N-Hydroxy succinimide as reducing and stable ligands, respectively. Compared with the previously reported strategy for the synthesis of metal nanoclusters, the proposed method is simple, green, and does not use any toxic organic reagents. Met-NHs-AuNCs showed the strongest red fluorescence at 634 nm. Methionine is one of the essential amino acids for cancer cell proliferation and metastasis and is one of the substrates of LAT1 transmembrane transporter.^{31–33} Therefore, the Met-NHs-AuNCs fluorescent probe synthesized in this study can target LAT1 on the surface of cancer cells for fluorescence imaging with high specificity. Several cancer cells incubated with Met-NHs-AuNCs for 2 hours showed bright red fluorescence, whereas normal cells (H9c2) showed no obvious phenomenon. In addition, the probe has strong red fluorescence, which has the advantages of eliminating the influence of cell fluorescence, less dispersion, and increased tissue penetration.³⁴ Therefore, Met-NHs-AuNCs has a promising application in targeted tumor imaging.

Methods and Materials

Materials

Methionine and Hydroxydatum natrium were obtained from the National Pharmaceutical Group Corporation (Shanghai, China). N-Hydroxy succinimide and HAuCl₄ were supplied by Aladdin Reagent (Shanghai) Co., Ltd. Cell culture

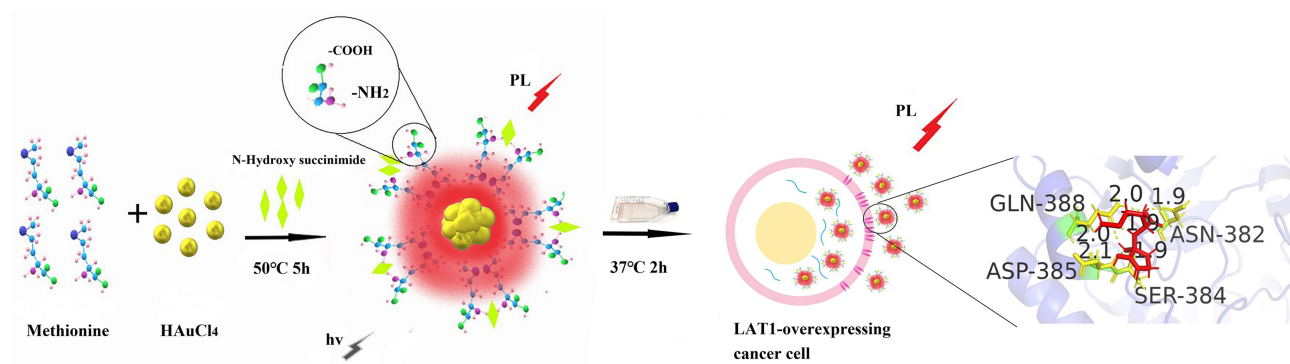


Figure 1 Met-NHs-AuNCs Au nanoclusters form and show high specificity in cancer cells.

medium and culture medium 1640 were purchased from GIBCO LTD. Fetal Bovine Serum (FBS) purchased ExCell Bio. Met, sodium hydroxide (NaOH), N-Hydroxy succinimide (NHs), PBS (phosphate buffer saline), and Amino acid were obtained from Shanghai Aladdin Bio-Chem Technology Co, Ltd, and were used as received without further purification. All chemicals were of analytical grade and prepared in ultrapure water (18.2 MΩ.cm). H9c2, AC16, A549, MCF-7, 4T-1 and HeLa cells were purchased from Shanghai Institute of Biochemistry and Cell Biology, Chinese Academy of Sciences (Shanghai, China).

Instruments

UV-vis absorption spectra of Met-NHs-AuNCs were recorded using a Shimadzu Corporation of Japan. Infrared spectroscopy of Met-NHs-AuNCs was recorded using NICOLET Is50 Fourier transform spectrometer (Thermo Fisher Scientific, US). Photoluminescent (PL) spectra were measured by FLS980 fluorescence spectrophotometer (Edinburgh Instruments, EI). Sample freeze-drying was used FD-1B type freeze dryer (Beijing Boyikang Experiment Instrument Co., Ltd). Photoluminescent (PL) spectra were measured by LitesizerTM500 nanoparticle size and potential analyzer. Fluorescence was recorded using inverted fluorescence microscope (Germany Laika Co., Ltd) equipped with a CCD camera. The size and dispersity measurements of the nanoclusters were performed with Tecnai G2 F20 field emission transmission electron microscope.

Synthesis of Au Nanoclusters

All glassware used in the experiment were thoroughly washed and dried with freshly prepared aqua regia. After mixing 1 mL (217.6 mmol L⁻¹) methionine with 0.485 mL chloroauric acid (6.4 mM) and 0.15 mL sodium hydroxide (0.5 mol L⁻¹) for 30 minutes, 0.375 mL of N-Hydroxy succinimide (7.5 mM) was added to react in 50 water bath. The solution was removed from the heater, cooled slowly to ambient temperature, and then centrifuged at 10,000 rpm for 10 minutes to discard large particles. Finally, the obtained Met-NHs-AuNCs were stored in a refrigerator at 4°C and kept away from light.

Characterization of Au Nanoclusters

The morphology and lattice of the samples were observed by transmission electron microscope. The excitation and emission spectra of Met-NHs-AuNCs of the synthesized near-infrared fluorescent probe were measured by fluorescence spectrometer. The ultraviolet-visible (UV-vis) absorption spectrum of the fluorescent probe was measured by UV-vis spectrophotometer. Quantum yield were measured on FLS980 fluorescence spectrometer. The surface groups of Met-NHs-AuNCs were analyzed by infrared spectrometer. A total of 200 μL probe solution was sent to the Malvern potential sample cell, and the surface charge of Met-NHs-AuNCs was measured by LitesizerTM500 nanoparticle size and potential analyzer.

Stability of Nanoclusters in Au Nanoparticles

Optical stability investigation: the Met-NHs-AuNCs were continuously tested for 3600 s under the excitation of 380 nm in the Time Course Parameters mode of the fluorescence spectrophotometer. Ion strength stability test: first, a series of concentrations of sodium chloride solution (0.01 MM-1.0 M) was prepared, and a fixed volume (ie, 1.5 mL NaCl solution) of different concentrations was added to 0.5 mL Met-NHs-AuNCs. Second, a negative control group was set up, mixed, and placed at room temperature in the dark for 30 min. Finally, the solution was transferred for fluorescence spectrum scanning, and each group concentration was repeated three times. PH stability test: first, a series of pH containing PBS buffer solution (pH3-11) was prepared, and a fixed volume of 1.5 mL PBS solution with different pH values was added to 0.5 mL Met-NHs-AuNCs. Then, the PBS solution was mixed and placed at room temperature in the dark for 30 min. Finally, the solution was scanned by fluorescence spectrum, and each group concentration was repeated three times.

The effects of common cations on the fluorescence of the Met-NHs-AuNCs were determined by testing NaCl, KCl, Zn(NO₃)₂, H₂PO₄⁻. For cell imaging, the effects of common cellular substances, including L-His, Lysine, L-Ascorbic acid, Glucose, Urea, on the fluorescence stabilities of the Met-NHs-AuNCs were, respectively, investigated. The concentration of all common substances is 1 mM. In addition, in order to prove that the fluorescence intensity of the probe is dose-dependent, we carried out fluorescence titration experiments. The detection limit is one of the important

bases to evaluate the performance of the probe. We calculated the detection limit of fluorescence according to the method in the literature.³⁵

Cytotoxicity Assay

MTT (3-(4,5-dimethyl-2-thiazolyl)-2,5-diphenyl-2-H-tetrazolium bromide) assay was performed to measure the cytotoxicity of Met-NHs-AuNCs to the normal target cells. H9c2 cells and AC16 cells were separately seeded in 96-well plates (7×10^3 cells/well) and incubated in the incubator for 24 hours. Then, the original culture medium was changed to different concentrations (0, 15.63, 31.25, 62.5, 125, 250, 500, 1000, 2000, 4000 $\mu\text{g/mL}$). After incubating for 24 hours, cells were treated with 100 μL of MTT solution (0.5 mg/mL). After another 4 hours of incubation, the medium containing MTT was cleared out with care and 150 μL of DMSO was used to dissolve the purple crystals in each well. After the reaction for 10 minutes, the absorbance was measured at 490 nm with an enzyme label. Cell viability % = $(\text{OD of test wells} - \text{OD of medium control wells}) / (\text{OD of untreated wells} - \text{OD of medium control wells}) \times 100\%$, OD denotes the optical density.

Cell Culture and Fluorescence Microscopy Imaging

Lung cancer cells (A549), breast cancer cells (MCF-7), mouse breast cancer cells (4T-1), and cervical cancer cells (HeLa) were cultured in 1640 culture medium, and cell blast suspension was added into 75 cm^2 culture flask and cultured in 37°C 5% CO_2 incubator. Hepatoma cells (HepG2), [Human hybrid] epithelioid cells (AC16) and cardiac myocytes (H9c2) were inoculated in DMEM culture medium containing 10% FBS, added to a 75 cm^2 culture flask, and cultured in a 37°C 5% CO_2 incubator. When the cells are in good condition, the cells reach the logarithmic phase when they cover 90% of the bottom area of the culture bottle, and the cells are plated for imaging. All cells were seeded in confocal dishes with a density of 2×10^4 cells per well. After overnight culture, 2 mL of synthetic fluorescent probe cell culture solution suspension was added and cultured in a 37°C 5% CO_2 incubator for 2 hours, then sucked off the supernatant and washed it with PBS for three times. After treatment, the targeted imaging between the near infrared fluorescent probe Met-NHs-AuNCs and the cell line on the cell imager was observed.

Molecular Docking Studies

The docking studies were carried out with Sybyl X-2.1.1. The PDB structure of LAT1 was selected from the Protein Database (RCSB PDB, the domain from human LAT1 (PDB ID:6IRT)). The PDB structure file was imported to Sybyl to generate active pocket based on Ligand mode, and the target protein was saved in SFXC format after optimization. All other parameters were in Sybyl software default value. LAT1 protein preparation step involved energy optimization and the addition of hydrogen and electric charge. The C_Score consistency evaluation scoring function of Surflex-Dock molecular docking module was used to score the interaction between active components and target protein LAT1. The larger the C_Score is, the better the affinity between the probe and LAT1 will be.

Results

Synthesis of Met-NHs-AuNCs

Met-NHs-AuNCs were prepared by using methionine as reductant and stabilizer, and then stabilizer N-Hydroxy succinimide was added. After mixing by suspension instrument, the solution was moved to a constant temperature instrument at 50°C for 5 h. After the reaction, the temperature was cooled to room temperature, and then the Met-NHs-AuNCs fluorescent probe was prepared by centrifugation. Met-NHs-AuNCs showed strong fluorescence emission at 634 nm, and the best excitation wavelength is 380 nm (Figure 2A). The Stokes shift of Au nanocrystals is calculated as 254 nm. This large Stokes shift may be caused by the formation of a luminescent Au (I) - mercaptan complex or a polynuclear Au (I) cluster, in which the hybrid S-Au transfer state participates in the luminescence transition.³⁶ The solution is yellowish at room temperature (Figure 2A-a) and emits strong red fluorescence under ultraviolet light excited by 365 nm (Figure 2A-b). The absolute quantum yield of Met-NHs-AuNCs in the aqueous solution was 3.35%.

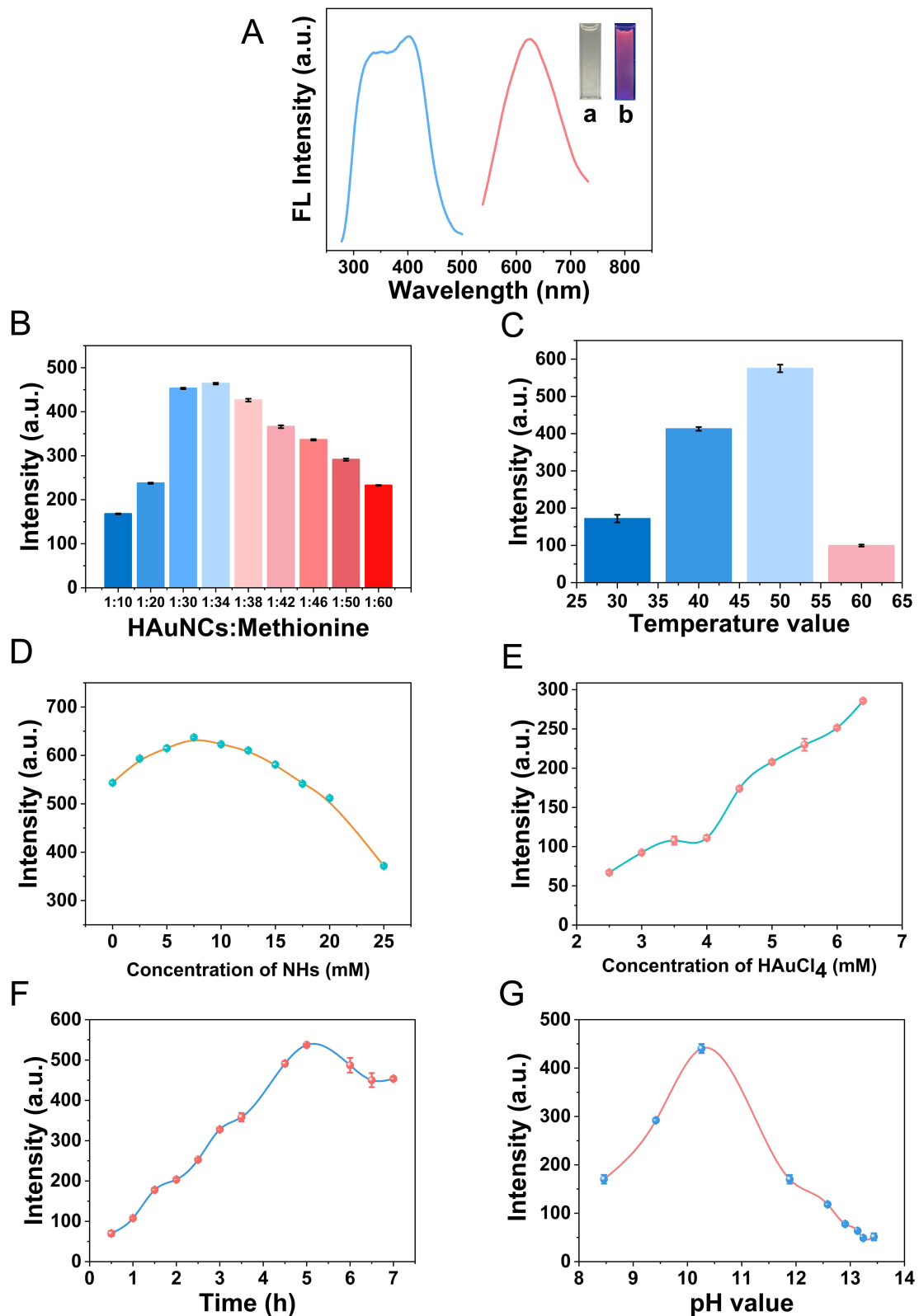


Figure 2 Optimization diagram of Met-NHs-AuNCs preparation conditions. (A) Fluorescence excitation and emission spectra of Met-NHs-AuNCs. (B) Optimization diagram of methionine chloroauric acid ratio. (C) Optimization of incubation temperature. (D) Optimization diagram of NHs concentration. (E) Optimization diagram of chloroauric acid concentration. (F) Optimization diagram of reaction time. (G) Optimization diagram of reaction pH.

In order to optimize the fluorescence intensity of Met-NHs-AuNCs, we investigated the optimum reaction concentration and the most suitable reaction conditions among the components. The concentration ratio of methionine-chlorauric acid was optimized separately, and chlorauric acid (0.485 mL, 2.5 mM) was fixed, methionine volume was 1 mL, and the concentration ratio was 1:10, 1:20, 1:30, 1:34, 1:38, 1:42, 1:46, 1:50, and 1:60, mixed with the same (0.15 mL, 0.5 M) NaOH reaction for 30 min. Next, N-Hydroxy succinimide (0.375 mL, 10 mM) was added to react in 50 water bath for 4 hours, and fluorescence intensity was measured (Figure 2B). The optimal ratio of methionine to chlorauric acid was 1:34, and the fluorescence intensity gradually increased with the increase of chlorauric acid ratio. When the concentration ratio was 1:34, the fluorescence intensity was the highest and an inflection point appeared. Then, the system temperature and concentration of N-hydroxy succinimide, chlorauric acid concentration, reaction time, and pH were optimized (Figure 2C–2). According to the optimization results, we selected 1 mL, 217.6 mM methionine, 0.485 mL of 6.4 mM chlorauric acid and 0.15 mL of 0.5 M Sodium hydroxide in stirring, mixed at room temperature for 30 minutes, then added N-Hydroxy succinimide of 0.375 mL and 7.5 mM, and incubated at 50°C for 5 h as the best preparation condition.

Characterization of Met-NHs-AuNCs

The morphology and lattice of Met-NHs-AuNCs were studied by transmission electron microscope (TEM). TEM analysis indicates the uniform morphology of Met-NHs-AuNCs (Figure 3A), and the average core size is 2.55 nm (Figure 3B). High-resolution transmission electron microscope images (Figure 3A) show individual Au nanoparticles with 0.232 nm lattice stripes that correspond to the (111) lattice plane of Au nanoparticles and confirm the crystal structure of metallic Au.³⁷

The optical properties of AuNCs were studied by UV-vis absorption spectra. As shown in Figure 3C, the spectra of the prepared Au nanoparticles show an insignificant absorption peak and do not have the characteristic surface plasmon resonance peak of the larger Au nanoparticles (around 520 nm), thereby suggesting that Met-NHs-AuNCs show similar molecular properties that differ from relatively large Au nanoparticles.³⁸ In addition, Met-NHs-AuNCs have an absorption peak at 260 nm. In contrast, no peak is observed at 260 nm in the absorption spectra of pure methionine, chlorauric acid, and Met-AuNCs, whereas N-Hydroxy succinimide has a weak absorption at 260 nm. The absorption peak of Met-NHs-AuNCs at 260 nm corresponds to the $n \rightarrow \pi^*$ transition of C=O and C-N in NHs structure, which may be caused by the increase in absorption intensity due to the connection with the auxochrome -OH and -NH₂ in methionine.³⁹

The surface groups of Met-NHs-AuNCs were analyzed by Nicolet Avatar 300 Fourier transform infrared spectrometer. In the FT-IR spectra, the peak at 1583 cm⁻¹ may be $\nu_{as}\text{NH}_3^+$ (N-H stretching vibration), and the peak at 1506 cm⁻¹ may be $\nu_{as}\text{COO}^-$ (C=O stretching vibration). In FT-IR spectra of Met and Met-AuNCs, only C-S stretching vibration (600–800 cm⁻¹) is observed. The $\nu_{as}\text{NH}_3^+$ and $\nu_{as}\text{COO}^-$ of Met did not shift or disappear in the Met-AuNCs (Figure 3D). Therefore, the sulfur atom of methionine, rather than -NH₂ and -COOH groups, is involved in the bonding of Met-AuNCs.^{40,41} As shown in Figure 3E, the peak near 1509 cm⁻¹ is produced by the C=O stretching vibration of methionine -COO⁻. The intensity and position of the peak do not change, thereby proving that -COO⁻ is not produced in the system, that is, the C-N bond of N-Hydroxy succinimide is not hydrolyzed to form succinic acid and still maintains the five-membered ring structure. The stretching vibration peak signal of hydroxyl O-H (3428 cm⁻¹) that corresponds to Met-NHs-AuNCs was increased significantly and far exceeded the superposition of the stretching vibration peak signal of N-Hydroxysuccinimide at 3421 cm⁻¹, suggesting the formation of -O-H structure. The peak of 1664 cm⁻¹ is the C=O stretching vibration peak of N-Hydroxysuccinimide, whereas the corresponding position of Met-NHs-AuNCs does not superimpose the carbonyl signal peak of NHs. Meanwhile, Met-NHs-AuNCs showed distinct peaks at 1580, which are ascribed to the $\nu_{as}\text{NH}_3^+$. However, the peak signal of -N-H stretching vibration (1571 cm⁻¹) of N-hydroxysuccinimide itself was weak, which might be caused by the peak superposition of the C=O stretching vibration of N-Hydroxy succinimide moving to low wave number, which is inferred to be the nucleophilic addition reaction of -NH₂ of methionine and -C=O group of N-Hydroxy succinimide on Met-AuNCs, resulting in the formation of amide structure -CO-NH₂. The aforementioned speculation also supports the cause for the increase in O-H stretching vibration (3428 cm⁻¹) peak signal. Combined with the results of UV spectrum analysis, it was verified again that -C=O in the structure of N-Hydroxysuccinimide was connected with the chromophore -NH₂ in methionine.

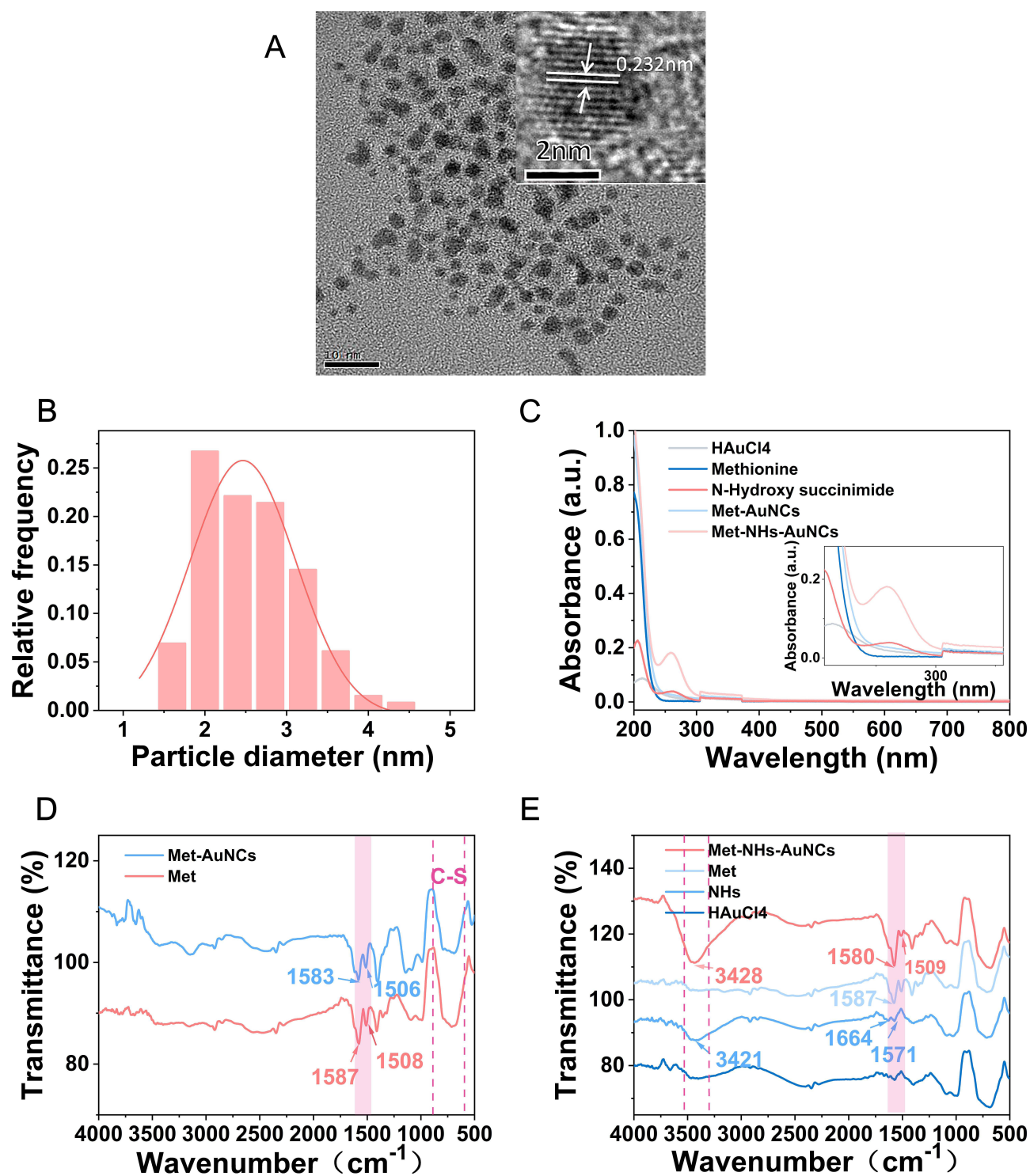


Figure 3 Characterization of Met-NHs-AuNCs. **(A)** TEM and high-resolution TEM of AuNCs prepared (inset). **(B)** Histogram of particle size distribution of AuNCs. **(C)** UV-vis absorption spectra of Met-NHs-AuNCs and its single component. **(D)** Comparison of infrared spectra of Met-AuNCs and Met. **(E)** Infrared spectra of Met-NHs-AuNCs and single component.

Stability of Fluorescent Met-NHs-AuNCs

The high stability of fluorescent nanomaterials is an important factor in evaluating their practical application. The zeta potential of Met-NHs-AuNCs solution was detected. By using ultrapure water as solvent, the average surface potential

was $-38.34 \text{ mV} \pm 0.69 \text{ mV}$. Met-NHs-AuNCs solution was negatively charged, and the synthesized Au nanoclusters were proven to be stable.

The fluorescence intensity after 3600 s was 105.34% of the initial intensity, thereby indicating the excellent optical stability of Met-NHs-AuNCs (Figure 4A). In addition to optical stability, the stability of ionic strength is also very important. With the increase in the concentration of sodium chloride, the fluorescence intensity of Met-NHs-AuNCs increased slightly at first and then decreased (Figure 4B). Meanwhile, the fluorescence intensity of the prepared probe was 85.68% of the initial intensity even at high ionic strength (1 M NaCl), which shows that Met-NHs-AuNCs have excellent ionic strength stability. In addition, the pH stability of the probe was also tested. As shown in Figure 4C, under various pH values from 3 to 11, the fluorescence intensity curve of Met-NHs-AuNCs at 634 nm fluctuates slightly, indicating that Met-NHs-AuNCs have relatively high pH stability. Due to its high stability, the synthesized Met-NHs-AuNCs fluorescent probe can be extended for practical applications. As shown in Figure 4D, common cellular substances did not give rise to radical changes in the PL intensity of the Met-NHs-AuNCs. These results revealed that the fluorescent Met-NHs-AuNCs are quite stable; thus, they are promising for biological applications. To ensure the sensitivity of the probe, we evaluated changes in fluorescence intensity in the presence of Met-NHs-AuNCs at different concentrations. The fluorescence intensity of Met-NHs-AuNCs gradually increased with the increase in concentration, showing a concentration dependence, as shown in Figure 4E. The fluorescence quenching factor $(F-F_0)/F_0$ was plotted against Met-NHs-AuNCs ion concentration. The acquired results showed the appropriate linearity ranges of R^2 value 0.98841, LOD value 1.66×10^{-4} mM (Figure 4F).

In vitro Imaging of Near-Infrared Fluorescent Probe

Due to the advantages of simple synthesis method, green synthetic reagent, and high sensitivity, Au nanoclusters have been widely used in cancer cell imaging.⁴² Met-NHs-AuNCs fluorescent probe contains methionine, which can target the overexpressed receptor LAT1 on the surface of cancer cells.⁴³ At the same time, through the network pharmacology Sybyl X molecular docking software, the consistency evaluation showed that the C_Score score of Met-NHs and LAT1 was 5, which had a high score evaluation and had a good interaction with the receptor LAT1 target and binds to the surface of LAT1. Therefore, the fluorescence imaging capability of Met-NHs-AuNCs fluorescent probe for carcinoma cells was investigated. We tested the toxicity of the Met-NHs-AuNCs to normal cells H9c2 and AC16 by MTT method. As shown in Figure 5A and B, the Met-NHs-AuNCs had little effect on the cell activity concentrations ranging from 15.63 to 2000 $\mu\text{g/mL}$ on cells (H9c2 and AC16). We first studied the fluorescence imaging of cervical cancer cell HeLa and cardiomyocyte H9c2 by Met-NHs-AuNCs and followed the imaging process with a fluorescence microscope. After incubation with the probe for 2 hours, HeLa cells showed strong red fluorescence. For comparison, normal H9c2 cells showed no obvious fluorescence after being incubated with the same volume of fluorescent probe for 2 hours (Figure 5C). The results showed that HeLa and H9c2 showed different fluorescence intensities, indicating different expression levels of LAT1 on their surfaces and the possibility of imaging cancer cells. In order to verify the targeted imaging of fluorescent probes, we used the competitive uptake experiment of methionine (Met) and Met-NHs-AuNCs. For the experimental group, HepG2 cells were pretreated with methionine (217.6 mM) for 2 h, and then incubated with fluorescent probes. For the control group, HepG2 cells were only incubated with the probe. Compared with the control group, the fluorescence signal of the experimental group was significantly weakened (Figure 5D).

In order to further explore the wide applicability of the fluorescent probe for cancer cell imaging, A549, MCF-7, HeLa, 4T-1, HepG2 and AC16 cells in the laboratory were incubated with Met-NHs-AuNCs for targeted cancer cell imaging. Under the same conditions as HeLa cells, all five cancer cells showed strong red fluorescence after incubation with Met-NHs-AuNCs (Figure 6). These results suggest that Met-NHs-AuNCs can distinguish normal cells from cancer cells and can be used for targeted imaging of cancer cells.

Discussions

This study indicates that (1) methionine and N-Hydroxy succinimide can be successfully combined with Au nanoclusters and their solutions emit strong red fluorescence under 365 nm UV excitation. (2) Met-NHs-AuNCs showed high stability in different environments. (3) The selective uptake of the probe by cells was attributed to the interaction between the probe and

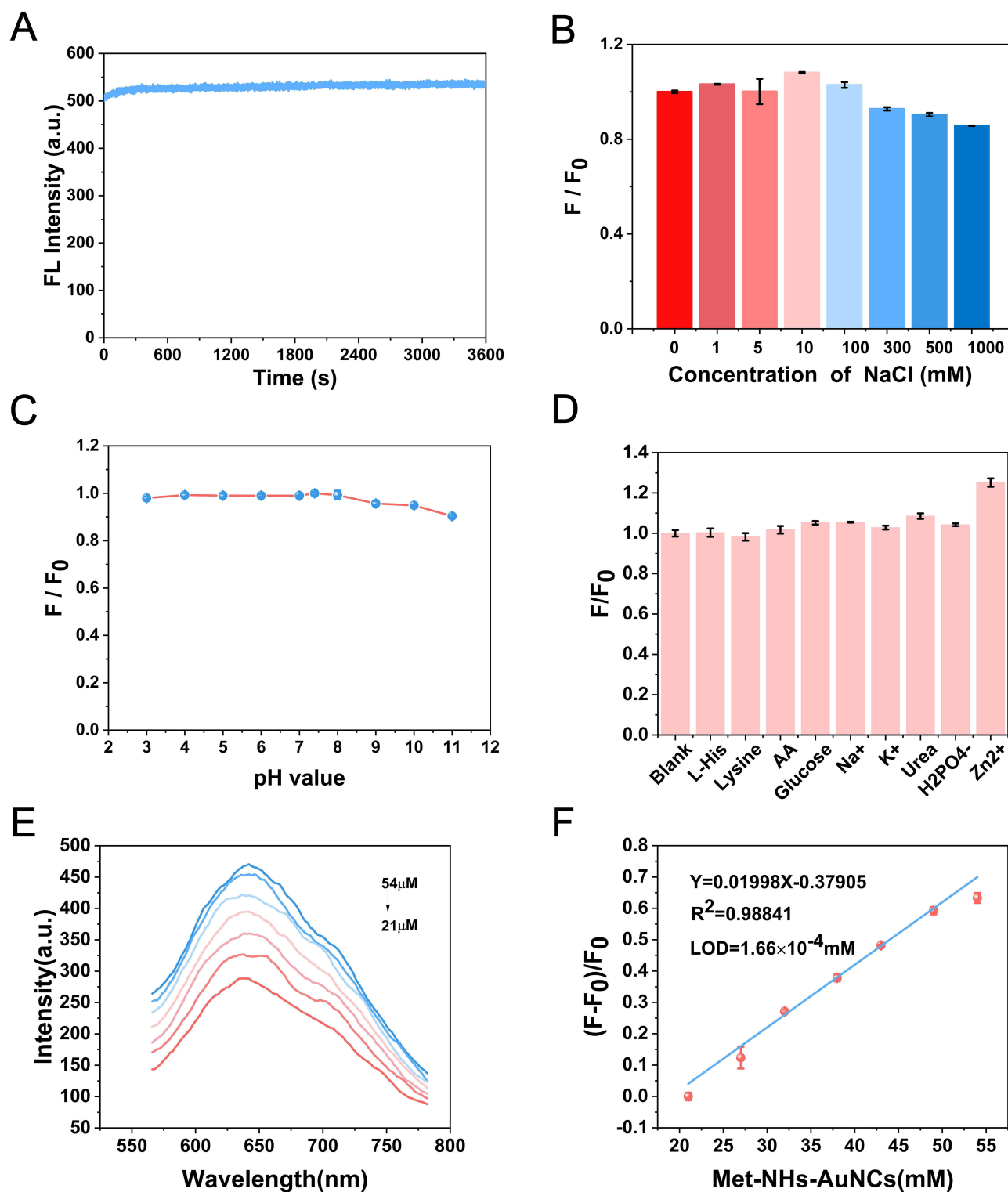


Figure 4 (A) Relationship between fluorescence emission intensity of Met-NHs-AuNCs in 634 nm and excitation time ($\lambda_{\text{ex}}=380$ nm). (B) Effect of different concentrations of NaCl on the fluorescence stability of Met-NHs-AuNCs. (C) Effect of different pH on the fluorescence stability of Met-NHs-AuNCs. (D) Fluorescence stability of Met-NHs-AuNCs in the presence of different environments. (E) Fluorescence spectrogram ($\lambda_{\text{ex}}=380$). (F) Changes upon increasing addition of Met-NHs-AuNCs concentration monitored using Luminoscope.

LAT1 receptor. (4) Met-NHs-AuNCs can distinguish between normal and cancer cells and can be used for targeted imaging of cancer cells. Previous studies have shown that Au nanoclusters exhibit fluorescent properties that can be used to easily track them in biological systems. Gold nanoclusters are non-toxic and stable in body fluids. Also, due to their small size (2–3

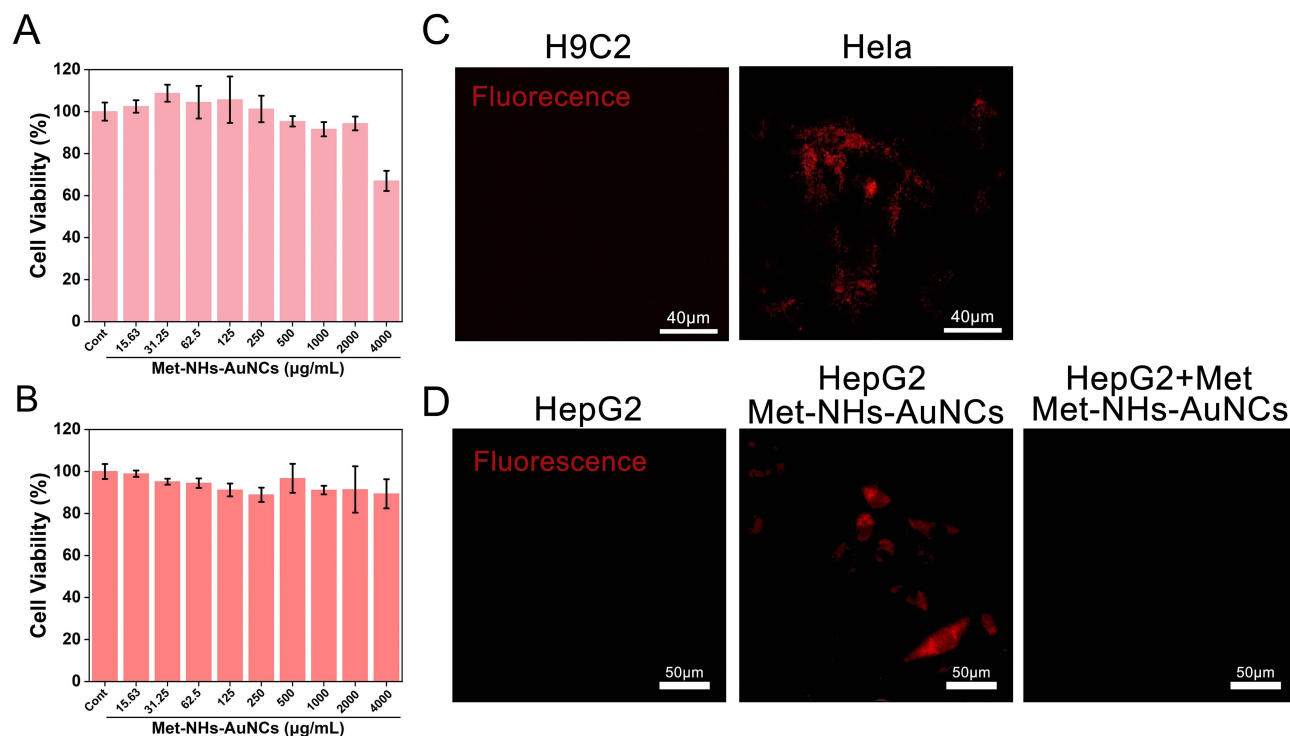


Figure 5 (A) Cell viability tests of H9c2 cells. (B) Cell viability tests of AC16 cells. (C) Fluorescence imaging of HeLa cells and H9c2 cells. (D) Selective imaging of HepG2 cells.

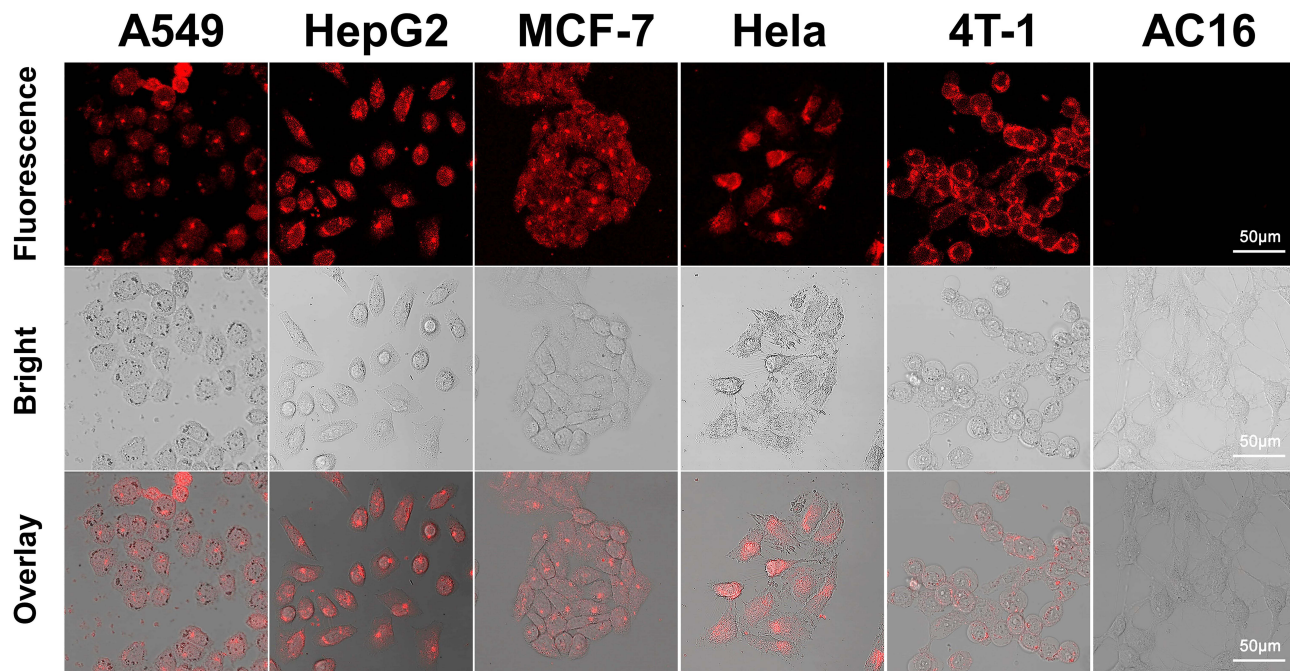


Figure 6 Cell imaging of A549, HepG2, MCF-7, HeLa, 4T-1 and AC16 incubated with Met-NHs-AuNCs for 2 hours.

nm), they interact with living systems in a different way and do not trigger any immune response. Therefore, we aim to take advantage of the benefits of gold nanoclusters to improve the sensitivity and selectivity of tumor imaging with a view to developing targeted tumor fluorescence imaging materials that specifically recognize overexpressed receptors that enter tumor cells.⁴⁴ Therefore, in this study, Au nanoclusters (Met-NHs-AuNCs) were designed and prepared reduced and

protected by methionine (Met) and N-Hydroxy succinimide (NHs) as fluorescent probes, and characterized and studied the stability of the probes. Through a series of studies, the prepared fluorescence probe has excellent properties such as large Stokes shift, strong red fluorescence emission, low background, high stability and selectivity, and can be used as a candidate for cancer cell imaging. Au nanomaterials are ideal materials for biological imaging because of their good biocompatibility, simple preparation and low price. We docked Met-NHs-AuNCs with LAT1 by using Sybyl X 2.1.1 software, selected high precision mode Surflex-Dock, and scored the structural conformation of probe and cancer cell overexpression receptor LAT1 more reasonably and accurately by using the consistency evaluation function C_Score, which integrates D_Score, PMF_Score, G_Score and Chem_Score functions. The C_Score of Met-NHs and LAT1 is 5, indicating that the probe has high affinity with LAT1 and binds to the surface of LAT1, so it has specific cancer cell or tissue imaging ability. Through the competitive experimental study of Met and Met-NHs-AuNCs, it is concluded that the targeting ability of Met-NHs-AuNCs is related to the interaction of LAT1, which is overexpressed on the surface of cancer cells. Due to the recognition of LAT1 transporter, the Met-NHs-AuNCs synthesized in this study can distinguish normal cells from cancer cells, showing strong red fluorescence in cancer cells (MCF-7, HepG2, HeLa, A549, 4T-1) while showing no fluorescence in normal cells. It has high targeting and sensitivity.

Conclusions

In summary, the synthesized Met-NHs-AuNCs red fluorescence probe has high specificity and can minimize the interference of autofluorescence of cells and tissues. Met-NHs-AuNCs are expected to be used in the diagnosis of clinical tumors.

Data Sharing Statement

Data will be made available on request.

Acknowledgments

The authors gratefully acknowledge the financial support provided by the National Science and Technology Planning Project [grant numbers 81973558, 22074017] and the key project supported by the Natural Science Foundation of Fujian Province, China [grant number 2021J02033] and the Fujian Provincial Natural Science Foundation [grant number 2021J01683].

Author Contributions

All authors made a significant contribution to the work reported, whether that is in the conception, study design, execution, acquisition of data, analysis and interpretation, or in all these areas; took part in drafting, revising or critically reviewing the article; gave final approval of the version to be published; have agreed on the journal to which the article has been submitted; and agree to be accountable for all aspects of the work.

Disclosure

The authors declare that they have no known competing financial interests or personal relationships that could have appeared to influence the work reported in this paper.

References

1. Siegel RL, Miller KD, Fuchs HE, Jemal A. Cancer statistics, 2022. *CA Cancer J Clin.* 2022;72(1):7–33. doi:10.3322/caac.21708
2. Tyson DM, Chavez MN, Lake P, et al. Perceptions of prescription opioid medication within the context of cancer survivorship and the opioid epidemic. *J Cancer Surviv.* 2021;15(4):585–596. doi:10.1007/s11764-020-00952-1
3. Schiffman JD, Fisher PG, Gibbs P. Early detection of cancer: past, present, and future. *Am Soc Clin Oncol Educ Book.* 2015;57–65. doi:10.14694/EdBook_AM.2015.35.57
4. Zhang Y, Wang J. Targeting uptake transporters for cancer imaging and treatment. *Acta Pharm Sin B.* 2020;10(1):79–90. doi:10.1016/j.apsb.2019.12.005
5. Pierce MC, Javier DJ, Richards-Kortum R. Optical contrast agents and imaging systems for detection and diagnosis of cancer. *Int, J, Cancer.* 2008;123(9):1979–1990. doi:10.1002/ijc.23858

6. Zhu N, Guo X, Pang S, et al. Mitochondria-immobilized unimolecular fluorescent probe for multiplexing imaging of living cancer cells. *Anal Chem.* 2020;92(16):11103–11110. doi:10.1021/acs.analchem.0c01046
7. Cui C, Chakraborty K, Tang XA, et al. A lysosome-targeted DNA nanodevice selectively targets macrophages to attenuate tumours. *Nat Nanotechnol.* 2021;16(12):1394–1402. doi:10.1038/s41565-021-00988-z
8. X-y H, J-j L, Yang Z-W, Zhang J, Wang H-S. Fluorescent intracellular imaging of reactive oxygen species and pH levels moderated by a hydrogenase mimic in living cells. *J Pharm Anal.* 2022;12(5):801–807. doi:10.1016/j.jpaha.2022.05.007
9. Li T, Yang J, Ali Z, et al. Synthesis of aptamer-functionalized Ag nanoclusters for MCF-7 breast cancer cells imaging. *Sci China Chem.* 2017;60:370–376. doi:10.1007/s11426-016-0159-2
10. Demir B, Lemberger MM, Panagiotopoulou M, et al. Tracking hyaluronan: molecularly imprinted polymer coated carbon dots for cancer cell targeting and imaging. *ACS Appl Mater Interfaces.* 2018;10(4):3305–3313. doi:10.1021/acsami.7b16225
11. Baghban R, Afarid M, Soleymani J, et al. Were magnetic materials useful in cancer therapy? *Biomed Pharmacother.* 2021;144:112321. doi:10.1016/j.biopha.2021.112321
12. Joshy KS, Augustine R, Mayeen A, et al. NiFe₂O₄/poly(ethylene glycol)/lipid-polymer hybrid nanoparticles for anti-cancer drug delivery. *New J Chem.* 2020;44(42):18162–18172. doi:10.1039/d0nj01163k
13. Siddique S, Chow JCL. Application of nanomaterials in biomedical imaging and cancer therapy. *Nanomaterials.* 2020;10(9):1700. doi:10.3390/nano10091700
14. Gao Q, Zhang J, Gao J, et al. Gold Nanoparticles in Cancer Theranostics. *Front Bioeng Biotechnol.* 2021;9:647905. doi:10.3389/fbioe.2021.647905
15. Woo Y, Chaurasiya S, O’Leary M, et al. Fluorescent imaging for cancer therapy and cancer gene therapy. *Mol Ther Oncolytics.* 2021;23:231–238. doi:10.1016/j.omto.2021.06.007
16. Lamberts LE, Koch M, de Jong JS, et al. Tumor-specific uptake of fluorescent bevacizumab-IRDye800CW microdosing in patients with primary breast cancer: a Phase I Feasibility Study. *Clin Cancer Res.* 2017;23(11):2730–2741. doi:10.1158/1078-0432.CCR-16-0437
17. Nozaki S, Nakatani Y, Mawatari A, et al. ¹⁸F-FIMP: a LAT1-specific PET probe for discrimination between tumor tissue and inflammation. *Sci Rep.* 2019;9(1):15718. doi:10.1038/s41598-019-52270-x
18. Jiao J, Zhang J, Yang F, et al. Quicker, deeper and stronger imaging: a review of tumor-targeted, near-infrared fluorescent dyes for fluorescence guided surgery in the preclinical and clinical stages. *Eur J Pharm Biopharm.* 2020;152:123–143. doi:10.1016/j.ejpb.2020.05.002
19. Zhu S, Tian R, Antaris AL, et al. Near-infrared-II molecular dyes for cancer imaging and surgery. *Adv Mater.* 2019;31(24):e1900321. doi:10.1002/adma.201900321
20. Zhang E, Luo S, Tan X, et al. Mechanistic study of IR-780 dye as a potential tumor targeting and drug delivery agent. *Biomaterials.* 2014;35(2):771–778. doi:10.1016/j.biomaterials.2013.10.033
21. Luo S, Zhang E, Su Y, et al. A review of NIR dyes in cancer targeting and imaging. *Biomaterials.* 2011;32(29):7127–7138. doi:10.1016/j.biomaterials.2011.06.024
22. Das RS, Mukherjee A, Kar S, et al. Construction of red fluorescent dual targeting mechanically interlocked molecules for live cancer cell specific lysosomal staining and multicolor cellular imaging. *Org Lett.* 2022;24(32):5907–5912. doi:10.1021/acs.orglett.2c02114
23. Wang W, Ma Z, Zhu S, et al. Molecular cancer imaging in the second near-infrared window using a renal-excreted NIR-II fluorophore-peptide probe. *Adv Mater.* 2018;30(22):e1800106. doi:10.1002/adma.201800106
24. Xing Q, Wang X, Yan X, et al. Multifunctional butterfly-shaped cyanine dyes: aggregation-induced emission, high-contrast mechanochromic luminescence, mitochondrial-specific staining and tumor imaging. *Dyes Pigm.* 2021;88:109232. doi:10.1016/j.dyepig.2021.109232
25. Kanai Y. Amino acid transporter LAT1 (SLC7A5) as a molecular target for cancer diagnosis and therapeutics. *Pharmacol Ther.* 2022;230:107964. doi:10.1016/j.pharmthera.2021.107964
26. Holley RW. A unifying hypothesis concerning the nature of malignant growth. *Proc Natl Acad Sci U S A.* 1972;69(10):2840–2841. doi:10.1073/pnas.69.10.2840
27. Yan R, Zhao X, Lei J, Zhou Q. Structure of the human LAT1-4F2hc heteromeric amino acid transporter complex. *Nature.* 2019;568(7750):127–130. doi:10.1038/s41586-019-1011-z
28. Scalise M, Galluccio M, Console L, Pochini L, Indiveri C. The human SLC7A5 (LAT1): the intriguing histidine/large neutral amino acid transporter and its relevance to human health. *Front Chem.* 2018;6:243. doi:10.3389/fchem.2018.00243
29. Bhutia YD, Babu E, Ramachandran S, Ganapathy V. Amino acid transporters in cancer and their relevance to “Glutamine Addiction”: novel targets for the design of a new class of anticancer drugs. *Cancer Res.* 2015;75(9):1782–1788. doi:10.1158/0008-5472.Can-14-3745
30. Okano N, Naruge D, Kawai K, et al. First-in-human phase I study of JPH203, an L-type amino acid transporter 1 inhibitor, in patients with advanced solid tumors. *Invest New Drugs.* 2020;38(5):1495–1506. doi:10.1007/s10637-020-00924-3
31. Häfliger P, Charles RP. The L-type amino acid transporter LAT1-an emerging target in cancer. *Int J Mol Sci.* 2019;20(10):2428. doi:10.3390/ijms20102428
32. Shindo H, Harada-Shoji N, Ebata A, et al. Targeting amino acid metabolic reprogramming via L-type amino acid transporter 1 (LAT1) for endocrine-resistant breast cancer. *Cancers.* 2021;13(17):4375. doi:10.3390/cancers13174375
33. Fuchs BC, Bode BP. Amino acid transporters ASCT2 and LAT1 in cancer: partners in crime? *Semin Cancer Biol.* 2005;15(4):254–266. doi:10.1016/j.semcancer.2005.04.005
34. Das RS, Maiti D, Kar S, et al. Design of Water-soluble rotaxane-capped superparamagnetic, ultrasmall Fe₃O₄ nanoparticles for targeted NIR fluorescence imaging in combination with magnetic resonance imaging. *J Am Chem Soc.* 2023;145(37):20451–20461. doi:10.1021/jacs.3c06232
35. David CI, Prabakaran G, Sundaram K, et al. Rhodanine-based fluorometric sequential monitoring of silver (I) and iodide ions: experiment, DFT calculation and multifarious applications. *J Hazard Mater.* 2021;419. doi:10.1016/j.jhazmat.2021.126449
36. Zheng J, Zhou C, Yu M, et al. Different sized luminescent gold nanoparticles. *Nanoscale.* 2012;4(14):4073–4083. doi:10.1039/c2nr31192e
37. Deng HH, Zhang LN, He SB, et al. Methionine-directed fabrication of gold nanoclusters with yellow fluorescent emission for Cu(2+) sensing. *Biosens Bioelectron.* 2015;65:397–403. doi:10.1016/j.bios.2014.10.071
38. Maruyama T, Fujimoto Y, Maekawa T. Synthesis of gold nanoparticles using various amino acids. *J Colloid Interface Sci.* 2015;447:254–257. doi:10.1016/j.jcis.2014.12.046
39. Peng Y, Wang M, Wu X, et al. Methionine-capped gold nanoclusters as a fluorescence-enhanced probe for Cadmium(II) sensing. *Sensors.* 2018;18(2):658. doi:10.3390/s18020658

40. Sang F, Zhang X, Shen F. Fluorescent methionine-capped gold nanoclusters for ultra-sensitive determination of copper(II) and cobalt(II), and their use in a test strip. *Mikrochim Acta*. 2019;186(6):373. doi:10.1007/s00604-019-3428-3
41. Bian RX, Wu XT, Chai F, et al. Facile preparation of fluorescent Au nanoclusters-based test papers for recyclable detection of Hg²⁺ and Pb²⁺. *Sens Actuators B Chem*. 2017;241:592–600. doi:10.1016/j.snb.2016.10.120
42. Zheng Y, Wu J, Jiang H, et al. Gold nanoclusters for theranostic applications. *Coord Chem R*. 2021;431:213689. doi:10.1016/j.ccr.2020.213689
43. Li L, Di X, Wu M, et al. Targeting tumor highly-expressed LAT1 transporter with amino acid-modified nanoparticles: toward a novel active targeting strategy in breast cancer therapy. *Nanomedicine*. 2017;13(3):987–998. doi:10.1016/j.nano.2016.11.012
44. Purohit R, Singh S. Fluorescent gold nanoclusters for efficient cancer cell targeting. *Int J Nanomed*. 2018;13(T-NANO 2014 Abstracts):15–17. doi:10.2147/IJN.S125003

Drug Design, Development and Therapy

Dovepress

Publish your work in this journal

Drug Design, Development and Therapy is an international, peer-reviewed open-access journal that spans the spectrum of drug design and development through to clinical applications. Clinical outcomes, patient safety, and programs for the development and effective, safe, and sustained use of medicines are a feature of the journal, which has also been accepted for indexing on PubMed Central. The manuscript management system is completely online and includes a very quick and fair peer-review system, which is all easy to use. Visit <http://www.dovepress.com/testimonials.php> to read real quotes from published authors.

Submit your manuscript here: <https://www.dovepress.com/drug-design-development-and-therapy-journal>